71st International Astronautical Congress (IAC) – The CyberSpace Edition, 12-14 October 2020.


IAC-20-C1.1.4

# Extended Mission Options for the Lunar IceCube Low-Thrust Spacecraft by Leveraging the Dynamical Environment

**Bonnie Prado Pino[a]*, Robert Pritchett[b], Kathleen C. Howell[c], David C. Folta[d]**

[a] *PhD Candidate, School of Aeronautics and Astronautics, Purdue University, West Lafayette, IN 47906, USA*, bpradopi@purdue.edu
[b] *PhD Candidate, School of Aeronautics and Astronautics, Purdue University, West Lafayette, IN 47906, USA; currently, NASA Goddard Space Flight Center, Greenbelt, MD 20771, USA,* robert.e.pritchett@nasa.gov
[c] *Hsu Lo Distinguished Professor of Aeronautics and Astronautics, Purdue University, West Lafayette, IN 47906, USA*, howell@purdue.edu
[d] *NASA Goddard Space Flight Center, Greenbelt, MD 20771, USA,* david.c.folta@nasa.gov
* Corresponding Author

**Abstract**

Upon deployment as a secondary payload from the Artemis-1 spacecraft, Lunar IceCube (LIC) will transfer to an orbit in the lunar vicinity from which it will complete its primary science and technology demonstration objectives. The efficiency of LIC's low-thrust engine enables the spacecraft to pursue extended mission objectives; however, the low acceleration level available to LIC offers significant challenges for the design of orbits and transfers. This investigation suggests a framework for the construction of low-thrust transfers between multi-body orbits in the lunar vicinity for applications with the LIC acceleration level. Low-thrust transfers are computed to and from a variety of multi-body orbits that exist in the vicinity of the Moon, e.g., Lyapunov, distant retrograde, and halo orbits. The proposed methodology offers a strategy applicable not only to the LIC mission but extendable to other low-thrust missions in the lunar vicinity, whether the acceleration capabilities are greater or less than LIC, particularly when science objectives, line of sight constraints, or orbital determination requirements, necessitate the use of multi- body orbits. Cost-time efficiency transfer performance is assessed that demonstrates the flexibility of the framework and delivers a new variety of mission options for the LIC spacecraft.

## 1. Introduction

The renewed interest in developing cislunar space has enabled numerous proposals involving small spacecraft destined for lunar orbit. Most of these small vehicles utilize low-thrust propulsion technology, for example, the Lunar IceCube (LIC) spacecraft, a 6U CubeSat equipped with a 1.24mN maximum thrust engine [1]. These low-thrust levels offer new challenges in trajectory design.

This investigation expands on the trajectory design framework introduced by Pritchett, Howell and Folta [2,3], in which a baseline trajectory to transfer the LIC spacecraft from its Earth deployment state into a low lunar elliptical science orbit is explored. In this new investigation, the science orbit for the LIC primary mission is assumed to be a member of the Southern (S) $L_2$ family of Near Rectilinear Halo Orbits (NRHOs); a variety of potential extended mission options is explored. Design flexibility enables the LIC spacecraft to further investigate the cislunar region, by moving between a set of multi-body orbits in the lunar vicinity, while operating under the constraint of reduced propellant due to the completion of the primary science and technology demonstrations objectives.

The proposed design approach splits the Lunar IceCube trajectory into three phases: phase I transfers the spacecraft from the Earth deployment state to a $L_2$ Northern (N) halo staging orbit in the lunar vicinity; phase II explores the path from the staging orbit to the NRHO science mission orbit; and, phase III investigates the possibilities of extended mission applications to other multi-body orbits in the lunar region, including but not limited to, Low Lunar Orbits (LLOs), Distant Retrograde Orbits (DROs), and other members of the halo family of orbits. Breaking the trajectory design into phases allows more flexibility, assures independent steps in the design framework, and simplifies the redesign process if the Earth deployment state is modified.

Phases I and II address the trajectory design problem by leveraging the dynamics in the Bicircular Restricted Four-Body Problem (BCR4BP) [4], while exploring the benefits of blending invariant manifolds from multi-body orbits with a Poincaré mapping strategy. All solutions are transitioned into a higher-fidelity ephemeris model, and a robust direct collocation algorithm is employed to provide locally optimal solutions. Preliminary design in the lower fidelity BCR4BP enables the gravitational force of the Sun to be smoothly incorporated to achieve part of the required energy change while avoiding the additional perturbations of a full ephemeris model.

The main challenges encountered during the design process in LIC's phase III are the large energy and plane changes required to transfer between multi-body orbits in the lunar vicinity given the limited low-thrust acceleration levels available. Thus, transfers in phase III are constructed by blending suitable arcs. A design methodology is developed that exploits such an orbit chaining strategy via two different approaches: (i) The spacecraft leverages the continuous evolution in amplitude and Jacobi constant values across families of multi-body periodic orbits to gradually modify its energy and inclination. Since the orbits of interest and their Jacobi constant values are native to the Circular Restricted Three-Body Problem (CR3BP), this force model—augmented by the influence of the thrust force—is employed by the algorithm to generate informed initial guesses that are converged to continuous solutions [5]. These transfer paths typically remain in the lunar vicinity (ii) The second approach utilizes long transits around the extended Earth-Moon system to achieve the required large plane changes. Results from both types of approaches are ultimately validated in a higher-fidelity ephemeris model that incorporates the gravitational influence of the Sun, the Earth and the Moon.

## 2. Dynamical Environment Models

The force models in the lower-fidelity CR3BP as well as the BCR4BP, offer an opportunity to approximate the higher-fidelity dynamics of a spacecraft in a multi-body regime, while exploiting the natural flows that are otherwise unavailable in simpler dynamical models (such as the Two-Body Problem (2BP)).

The CR3BP models the path of the spacecraft, $P_3$, under the influence of two primary bodies, $P_1$ and $P_2$, that are assumed to move in circular orbits about their mutual barycenter, $B_1$. The BCR4BP adds the gravitational attraction of a fourth primary body, $P_4$; $P_4$ and the $P_1 - P_2$ barycenter, $(B_1)$, are assumed to move in circular orbits about their mutual barycenter, $B_2$ [6].

However, the true motion of the celestial bodies is time-dependent, as is their gravitational influence on the motion of a spacecraft, resulting in the mission epoch being a critical quantity for the true modeling of a spacecraft trajectory. The inclusion of the ephemeris model represents these more complex dynamics. In this investigation, all celestial bodies are modeled as point masses, and perturbation influences in addition to gravity, such as, spherical harmonics effects, drag perturbations, or solar radiation pressure, are not incorporated in the dynamical models.

### *2.1 Low-Thrust n-body Ephemeris Model*

To represent the motion of a low-thrust spacecraft $(P_3)$ moving with respect to a primary body $(P_q)$ in a time-dependent system, under perturbations from the gravitational influences of $n$ additional nearby bodies, as represented in Figure 1; let $T$ represent the dimensional thrust acceleration magnitude, $M$ corresponds to the dimensional mass of the spacecraft, $M_j$ $(j = 1, \dots, n)$ is the dimensional mass of each perturbing body, and $\tilde{G}$ is the dimensional gravitational constant. The spacecraft's acceleration vector expressed in a J2000 inertial reference coordinate frame, centered on the primary body, is given by:

$$\ddot{\bar{r}}_{q3} = -\frac{\tilde{G}(M_3 + M_q)}{r_{q3}^3}\bar{r}_{q3}^3 + \tilde{G}\sum_{\substack{j=1 \\ j\neq q,3}}^{n} M_j\left(\frac{\bar{r}_{3j}}{r_{3j}^3} - \frac{\bar{r}_{qj}}{r_{qj}^3}\right) + \frac{T}{M_3}\hat{a}_T \qquad (1)$$

where the unit vector $\hat{a}_T$ represents the thrust orientation vector, the vector $\bar{r}_{q3}$ corresponds to the position vector from the spacecraft to the primary body, the vector $\bar{r}_{qj}$ is the position vector from each perturbing body to the primary, and the vector $\bar{r}_{3j}$ corresponds to the position vector from the spacecraft to each of the perturbing bodies.

The J2000 coordinate frame is an Earth-centered inertial reference frame where all directions are recorded on January 1st, 2000 at 12:00:00 Ephemeris Time (ET) (Julian Date: 2451545.0 ET) [7], in which the $x$-axis is directed along the vernal equinox, the $z$-axis is parallel to the Earth spin axis direction, and the $y$-axis completes the right-handed triad. The relative position quantities in Eqn. (1) associated with the gravitational bodies, are accessed via SPICE toolkits [8], and are computed from the NASA's Jet Propulsion Laboratory DE421 ephemerides data.

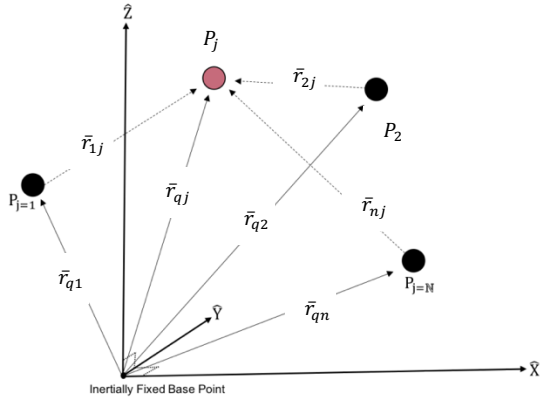


Fig. 1. Graphical representation of the n-body problem. Particle $P_j$ under the gravitational influence of $n-1$ attracting bodies

### *2.2. Roughness Parameters Technique*

One of the main challenges in the design of spacecraft transfer trajectories in the ephemeris model, is the

selection of the initial epoch [9]. Since the ephemeris model is a time-dependent system, in which the position of the celestial bodies is no longer assumed to be static (as it is the case for simplified force models), the epoch plays an important role as it dictates the correct phasing of the gravitational bodies in the dynamical model; Thus, selecting the correct epoch may aid in the convergence of a transfer solution; however, the efficiency of the corrections algorithm can decrease by selecting an epoch with the wrong phasing.

To reduce the sensitivity of the trajectory convergence in the ephemeris model to the initial epoch, the concept of a Roughness Parameter (RP) is introduced [5]. In its pure mathematical definition, the roughness parameter is a quantity used to assess the smoothness of a curve [10]. The smoothness is quantified by measuring the discontinuities along the path. A fully continuous path should yield a null RP and, as the path evolves into a piecewise continuous function, the RP value should increase. Thus, as discontinuities emerge, the RP value growths larger than zero.

In astrodynamics applications, the roughness parameter calculation in utilized in the generation of spacecraft trajectories in the ephemeris model. There are multiple ways to compute the RP value and the method selected depends on the type of variations, or the characteristics of the path, to be assessed. Assume that position is potted as a function of time. If the vertical characteristics of the profile are desired, then amplitude roughness parameters should be employed. If instead, the horizontal characteristics of the profile are sought, spacing roughness parameters are more useful. Lastly, a combination of vertical and horizontal characteristics of a profile can be evaluated by computing a hybrid roughness parameter.

In this investigation, the Root Mean Square (RMS) value of the profile for the magnitude of the position vector of the spacecraft relative to the central body, is employed as the roughness parameter measure. The process for leveraging this RP concept within the ephemeris model is accomplished as follows [5]:

1. For a selected initial epoch, propagate the trajectory initial guess, and discretize it into a finite number of points
2. Compute the magnitude of the position vector of the spacecraft relative to the central body
3. Compute the roughness parameter (RMS) value corresponding to that particular trajectory and epoch
4. Repeat steps 1 through 3 for a variety of different epochs
5. Select the initial epoch that yields the lowest RP value

Figure 2 depicts a sample representation for the magnitude of the position of a spacecraft in the vicinity of the Moon. The RMS value for this position profile is simply computed as:

$$RMS = \sqrt{\frac{1}{k}\sum_{i=1}^{k} p_i^2} \qquad (2)$$

where $k$ represents the number of discretization points, and $p_i, i = 1, \dots, k$ is the magnitude of the position vector at time $i$. The RMS value is straightforward to evaluate.

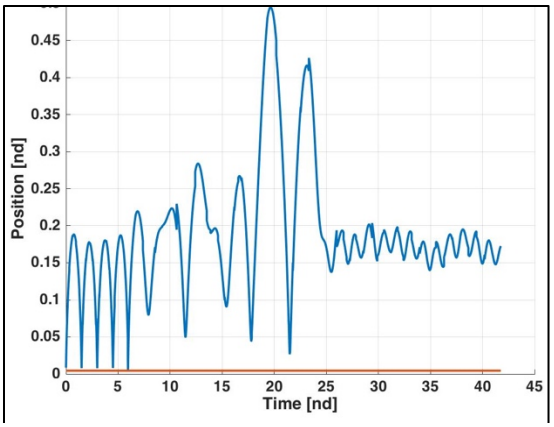


Fig. 2. Sample profile for the magnitude of the position vector of a spacecraft relative to the Moon, in a higher-fidelity ephemeris model, for a selected initial epoch. The red line represents the lunar radius.

While the RMS quantity is one of the most popular amplitude roughness parameter measures, there exist other options for amplitude parameters, for example, the maximum height of the profile, the amplitude density function, or the power spectral density function. Some of the most popular spacing roughness parameters include the measure of the number of peaks in the profile, and the number of inflection points.

## 3. Trajectory Design Framework

To develop a general framework for trajectory design for the Lunar IceCube (LIC) spacecraft, the process is divided into three phases; this division does not only facilitate the accommodation for modified Earth deployment state epochs in the primary mission, but also generalizes the search for extended mission applications that are independent of the arrival epoch of the LIC into its primary science mission orbit.

The LIC's primary mission is comprised of phases I and II [11], while the potential extended applications are investigated in phase III. Furthermore, this generalized trajectory design framework allows for the generation of two types of low-thrust transfer geometries. Trajectories with an exterior-type geometry correspond to paths that depart the vicinity of the Earth-Moon system to accomplish the required energy and plane changes, and later re-enter into the lunar region. The interior-type

geometries are those that remain within the lunar vicinity and accomplish the required energy and plane changes by leveraging the dynamical structures that exist within the simplified CR3BP and BCR4BP models.

### *3.1 Generation of Exterior Trajectories*

In this investigation, the proposed method for constructing initial guesses to deliver exterior-type geometries for low-thrust spacecraft trajectory is summarized in the diagram in Figure 3; The spacecraft originates in the vicinity of the libration point orbits in the CR3BP as represented for the Earth-Moon system. The strategy then varies for spacecraft pathways to link two stable orbits, two unstable orbits, or a combination.

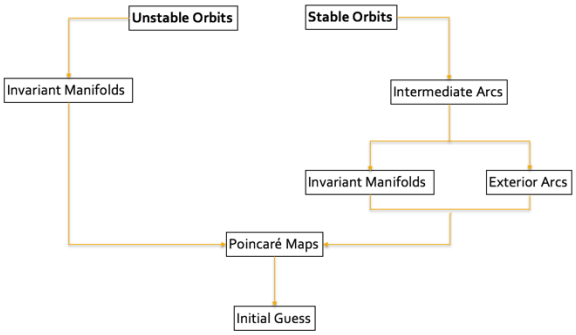


Fig. 3. Graphical representation of the algorithm for generation of exterior trajectories

Within the context of the CR3BP a periodic orbit is a solution to the nonlinear differential equations to represent the motion of the spacecraft as a closed periodic path. To analyze the stability of periodic orbits the model is formulated in terms of a set of linear variational equations [12,13]. The solution to this linear system is:

$$\delta\bar{x}(t) = \Phi(t, t_0)\delta\bar{x}(t_0) \quad (3)$$

where $\delta\bar{x}(t)$represents the variation in the state vector at time $t$, $\Phi(t, t_0)$ corresponds to the state transition matrix and $\delta\bar{x}(t_0)$ identifies the initial variations of the state vector. The eigenvalues of the monodromy matrix are the modes that dictate the linear behavior in the vicinity of a periodic orbit and, therefore, its stability.

The state vector in the natural CR3BP –that is, the system for which the low-thrust acceleration has not been incorporated–, is six-dimensional (three dimensions corresponding to the position elements, and three for the velocity components). Representing a periodic orbit as a fixed point, its stability is assessed via the monodromy matrix (i.e., the state transition matrix after precisely one period of the orbit). For a given location along the orbit, the monodromy matrix corresponding to each fixed point possesses six eigenvalues and a corresponding set of associated eigenvectors. Two eigenvalues, denoted the trivial pair, are always equal to one; the remaining four eigenvalues, denoted the nontrivial eigenvalues, occur as two reciprocal pairs, and are of the form $\lambda_i = a \pm b_j$, with $i = 1, \ldots, 4$ and $j = 1,2$, where $a$ and $b$ are real numbers. The linear stability of a periodic orbit is determined by considering the form and magnitude of each of the four nontrivial eigenvalues; there are two possible forms for each of the nontrivial pairs [13]:

- Complex roots, i.e., $\lambda_{1,2} = a \pm b_i$. If the roots lie on the unit circle, the solution is bounded – or marginally stable; a perturbed path neither approaches nor departs from the reference over time
- Real roots, i.e., $b = 0$ and $\lambda_1 = a$, $\lambda_2 = \frac{1}{a}$. These roots correspond to exponential growth or decay of the variation between the reference and perturbed paths over time

Following the schematic in Figure 3, if one or both of the departure and arrival orbits exhibit unstable behavior, a Poincaré map analysis is completed. Alternatively, if both orbits exhibit stable behavior, an alternate structure is sought as an intermediate arc, one that exist in the form of manifold structures or exterior-type periodic orbits, for example, resonant orbits, and drive the geometry of the final transfer.

Significant insight into the flow along a trajectory, is gained by reducing the dimension of the system such that implicit information is captured in a lower dimensional visual representation. Poincaré mapping is a very useful approach to effectively reduce the dimensionality of a dynamical system and allow for concise visualization of the flow. To construct such a map, a hyperplane or surface of section ($\Sigma^+$) is selected, at which crossings of a propagated trajectory for a variety of initial conditions, $\bar{x}_1$, are recorded. The mapping $\bar{x}_1 \rightarrow P(\bar{x}_1)$ is then termed the Poincaré map, and each time a propagation crosses the hyperplane, its information is recorded [14].

The generation of exterior trajectories for linking unstable orbits is then accomplished by propagating the branches from the invariant manifolds or from exterior resonant orbits and represent them on a map. The corresponding intermediate arcs are extracted for inclusion in the construction of an initial guess. An infinite number of possibilities exist for the selection of intermediate orbits –or arcs– and a few are examined in this investigation.

### *3.2 Generation of Interior Trajectories*

To compute interior trajectories, this investigation exploits an energy-informed adaptive sliding algorithm [5], that utilizes natural arcs in the CR3BP force model, within an orbit chaining framework, to construct initial guesses for low-thrust spacecraft trajectories between libration point orbits in the vicinity of the Moon, whether

the orbits are considered stable or unstable, based on the simple energy relationship

$$C_f = C_i + \sum_{j=1}^{N} \Delta C_j \quad (4)$$

where $C_f$ represents the energy of the arrival (final) orbit, $C_i$ corresponds to the energy of the departure (initial) orbit, and $\Delta C_j$ is the change in energy required to move from one orbit to the next, within the context of an orbit chaining framework. The orbit chaining framework [15] offers a flexible, yet robust approach to initial guess construction for low-thrust trajectory design in lower-fidelity force models. Since this strategy is not tied to a specific dynamical model, it is applicable within both the CR3BP and the BCR4BP to meet the needs of a given design problem.

The orbit chaining framework employs any type of dynamical structure. The main goal of the sliding algorithm strategy is, then, to identify natural dynamical structures, such as, periodic orbits or invariant manifold branches, to traverse the gaps in position and velocity space between a departure and an arrival orbit. The orbit chain is constructed following the six-steps below:

1. Analyze any dynamical structures that exist in the vicinity of the departure and arrival orbits
2. Select natural arcs that offer high-efficiency energy paths
3. Clip the sections of the arcs that best suit the transfer requirements and form an initial guess
4. Subdivide the initial guess for the trajectory into smaller segments and patch points
5. Stack additional revolutions of the initial and final orbits as appropriate
6. Define the control history by utilizing either a differential corrections process or an optimizer, to produce a converged solution

The previous steps outline the framework followed by the adaptive algorithm to construct locally optimal solutions via orbit chaining, by identifying and utilizing the minimum number of intermediate arcs that are necessary to pass through from the departure to the arrival orbits which subsequently produces and end-to-end transfer. The algorithm delivers the initial guess for the trajectory. The energy-informed adaptive sliding algorithm offers the capability to identify interior transfer geometries when manifolds arcs are not available, also representative of a spacecraft transferring between two stable orbits.

To estimate this minimum number of intermediate arcs, or minimum number of orbits in a chain, the method relies on a parametrization of the energy evolution for the families in consideration, along with the accessible region –in configuration space– provided by the thrust capabilities of the spacecraft. The goal is achieved by minimizing the following objective function:

$$J = \min_{N \in \mathbb{N}} \left\{ W_1 \left( \frac{1}{2} \sum_{j=1}^{N} \Delta C_j^2 \right) - W_2 ToF \right\} \quad (5)$$

This nondimensional objective function is comprised of two different terms: (i) an energy related term, that reduces the number of energy changes from one propagation arc along the transfer to the next; and (ii) a time-of-flight term, that accommodates the convergence of time-optimal trajectories. The weights associated with each of the individual terms are represented by $W_1$ and $W_2$, respectively, and aid in prioritizing the type of optimal transfer to be delivered. The energy of each intermediate orbit as reflected in the corresponding value of the Jacobi constant is represented by $C_j$, and $ToF$ is the total time-of-flight along the transfer.

Since the geometry of the converged solution relies heavily on the characteristics of the initial guess, there are an infinite number of options to slide through the space, i.e., to transfer between a departure and an arrival orbit; one such option is represented in Figure 5, where the energy-informed adaptive sliding algorithm is leveraged to identify the minimum number of intermediate orbits required in the construction of an initial guess for the generation of an interior-type trajectory from an NRHO to a DRO in the vicinity of the $L_2$ libration point. The adaptive sliding algorithm uses one of many metrics that are manipulated to determine the intermediate arcs, leaving room for a variety of other transfer geometries.

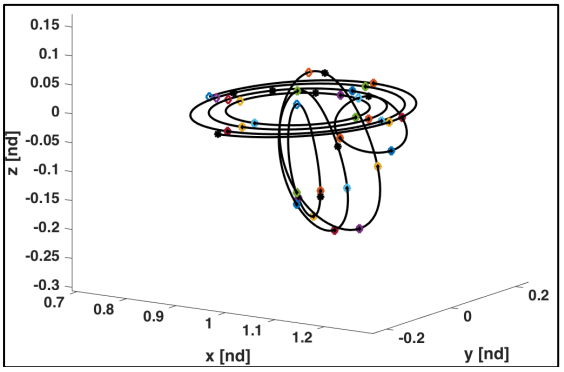


Fig. 5. Sample initial guess trajectory for an interior transfer from a $L_2$ S NRHO to a $P_2$ DRO in the CR3BP model, generated via the energy-informed adaptive sliding algorithm

## 4. LIC End-to-End Ephemeris Trajectories

The main challenge encountered in the design of the primary mission for the lunar IceCube (LIC) spacecraft is the large change in energy required to transfer from the high-energy deployment state near the Earth to the

science orbit. While the initial velocity of LIC relative to the Earth is less than the escape velocity, the subsequent ballistic path includes a flyby of the Moon that enables LIC to escape the Earth-Moon system, thus, resulting in an exterior-type trajectory. The strategy to initiate a low-thrust maneuver shortly after Earth deployment, prevents the spacecraft from escaping into heliocentric space. Such is the objective of phase I of the trajectory design process.

The candidate LIC science orbit for the primary mission as defined in this investigation, possesses an energy sufficiently low to ensure that the spacecraft is securely captured into the lunar vicinity for the duration of the primary mission. Designing this trajectory arc is the main focus of phase II.

Recording LIC's arrival epoch into its primary science mission orbit, along with the propellant consumption requirements, allows for the flexibility to further expand the mission into potential extended options, which is the objective of the phase III of the trajectory design strategy.

### *4.1 LIC Phase I: Earth Deployment to Lunar Staging Orbit*

Each time a new deployment state and epoch is selected, the baseline trajectory must be redesigned. Experience has demonstrated that varying the launch date can significantly impact the geometry of any trajectories that deliver LIC to the specified science orbit. Previous authors have investigated and designed transfer trajectories that deliver a CubeSat from an Earth deployment state to a multi-body orbit around the Moon [15, 16].

Timing discrepancies between the end of Phase I and the beginning of Phase II are eliminated by placing the spacecraft in a staging orbit near the Moon, until reaching the desired departure epoch. The selection of the appropriate staging orbit is based on identifying candidate orbits that offer invariant manifold structures, such that natural energy-efficient arcs are exploited. In this investigation, the selected staging orbit is a member of the $L_2$ N halo family of orbits.

By utilizing the dynamics of the BCR4BP, along with a robust optimization algorithm via direct collocation, an initial guess is generated that delivers LIC from its deployment state near the Earth, to a $L_2$ N halo staging orbit. This solution is then converged in a high-fidelity ephemeris model, resulting in the trajectory plotted in Figure 6. Red arcs correspond to thrust segments, and blue arcs represent segments where the engine is coasting. The spacecraft requires about 194 days from its Earth deployment state to the destination orbit, and it consumes 0.08 kg of its 14 kg initial mass, where a deployment epoch of March 1st, 2021 has been adopted for the ephemeris design.

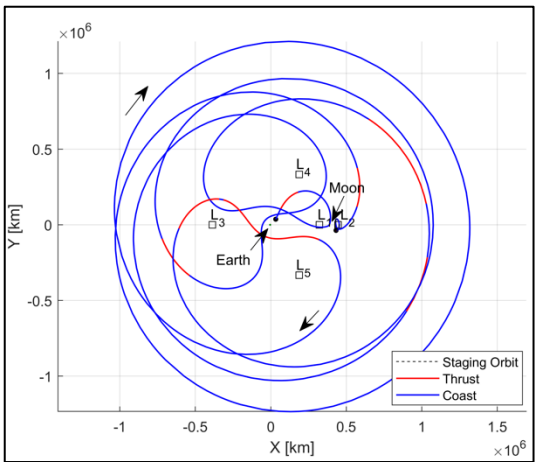


Fig. 6. Exterior transfer from the Earth deployment state to a $L_2$ N halo stating orbit in the ephemeris model. Red and blue arcs represent thrust and coasting segments, respectively

### *4.2 LIC Phase II: Lunar Stating Orbit to Science Mission Near-Rectilinear Halo Orbit (NRHO)*

A 9:2 synodic resonant $L_2$ Southern (S) Near Rectilinear Halo Orbit (NRHO) is considered in this investigation as an alternate candidate orbit for LIC's primary science mission; hence, generating suitable trajectories from the staging halo orbit from phase I to the 9:2 $L_2$ S NRHO is the goal of phase II. After examining the energy characteristics of the 9:2 $L_2$ S NRHO, the change in energy required to reach this orbit from the staging halo orbit does not necessitate a long low-thrust spiral, and a simple orbit chain approach is leveraged to achieve an interior-type trajectory between departure and destination. Within the context of the BCR4BP, one or more revolutions for each periodic orbit are stacked along the departure and arrival orbits, and the resulting initial guess appears in Figure 7. These arcs are discretized into patch points and segments, and a differential corrections process is employed to converge this initial guess into a feasible low-thrust solution, continuous in position, velocity and mass.

The control history for the initial guess in the BCR4BP is defined such that the thrust acceleration magnitude is set to zero, and the thrust orientation vector is pointed along the relative anti-velocity direction for all discretized segments. The fully converged solution in the BCR4BP is utilized as an initial guess for the higher-fidelity model, and optimized via a direct collocation approach, to produce the trajectory depicted in Figure 8 that corresponds to the LIC's path from the staging $L_2$ N halo orbit to the 9:2 $L_2$ S NRHO science orbit in a higher-fidelity ephemeris model that includes the gravitational attraction of the Sun, the Earth and the Moon.

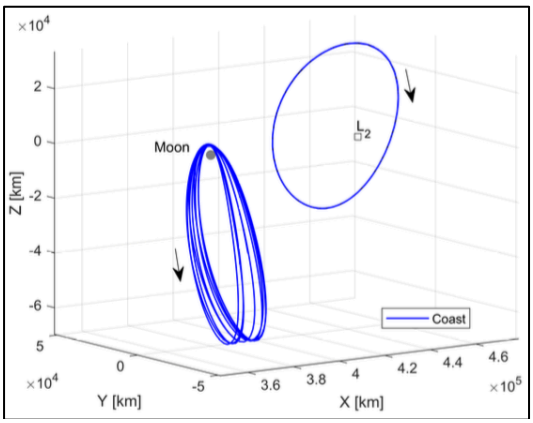


Fig. 7. Phase II initial guess trajectory in configuration space in the BCR4BP model. Multiple revolutions of the departure and arrival orbits are stacked via an orbit chaining approach

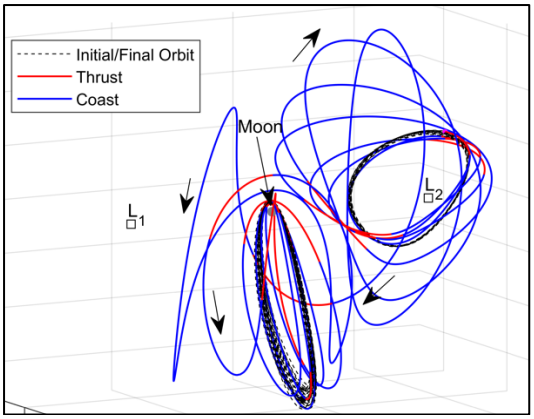


Fig. 8. Interior transfer from the $L_2$ N halo staging orbit to the $L_2$ S 9:2 NRHO science orbit in the ephemeris model. Red and blue arcs represent thrust and coasting segments, respectively

For a selected epoch of March 1st, 2021, in the ephemeris model, the spacecraft requires about four months to travel from the staging to the science orbit, and it consumes 0.2 kg of the available propellant mass. Other epochs for Earth deployment states are also considered in this investigation, two of which are summarized in Table 1. The performance of LIC's trajectories for phases I and II, in terms of propellant consumption and time-of-flight, for the two selected Earth departure epochs in the ephemeris model are studied. In both cases, the LIC spacecraft requires under 400 days to transfer from its deployment state near the Earth to the $L_2$ S 9:2 NRHO science orbit (i.e., combined phases I and II), and the propellant consumption is under 500 gr of the initial 14 kg. This performance enables the ability for the spacecraft to further explore alternative mission options, assuming a new initial mass of 13.6 kg, and a departure epoch of no earlier than January 1st, 2022, to allow for completion of the primary mission objectives.

Table 1. Summary of results for Phases I and II of LIC primary mission trajectory from Earth deployment state to science orbit

| | Performance | 09/06/20 | 03/01/21 |
|---|---|---|---|
| Phase I | $\Delta m\ [kg]$ | 0.10 | 0.08 |
| | $ToF\ [days]$ | 117.39 | 194.46 |
| Phase II | $\Delta m\ [kg]$ | 0.26 | 0.07 |
| | $ToF\ [days]$ | 173.92 | 173.92 |
| Total | $\Delta m\ [kg]$ | 0.36 | 0.14 |
| | $ToF\ [days]$ | 301.54 | 393.91 |

### *4.3 LIC Phase III: Potential Extended Missions*

After arriving on the science orbit dictated by the primary mission and summarized in phases I and II of the trajectory design framework, the LIC is expected to remain in the $L_2$ S 9:2 NRHO performing its science and technology demonstrations. The examples and ephemeris epochs examined in this investigation for completion of the primary mission, suggest that the spacecraft propellant reserve, to perform any potential extended mission application, is of 13.6 kg at best.

By leveraging the natural structures that exist within the CR3BP force model, and, utilizing an energy-informed adaptive algorithm to generate interior-type trajectories, a variety of different transfer from the $L_2$ S 9:2 NRHO to other multi-body orbits in the lunar vicinity are explored as possible candidates for LIC extended mission options. The initial guess for all transfers is generated within the context of CR3PB system, and later corrected in a higher-fidelity ephemeris model that includes the gravitational perturbations of the Sun, the Earth and the Moon. All transfers are locally optimal solutions generated via a Sequential Quadratic Programming (SQP) direct optimization scheme.

#### *4.3.1 Phase III.1: Transfer from a NRHO to a Lunar Distant Retrograde Orbit (DRO)*

Consider the design of a low-thrust spacecraft trajectory from a $L_2$ S 9:2 NRHO to a 70,000km-altitude Distant Retrograde Orbit (DRO) around the Moon. The design of this trajectory is particularly challenging, as both the departure and the arrival orbits are considered to be stable orbits in the Lyapunov sense. This stability characteristic suggests that there are no structures that depart or arrive into the orbits naturally, such as invariant manifold structures; hence, a creative strategy for generating informed initial guesses is required.

The orbit chaining framework within the context of the energy-informed adaptive algorithm provides such strategy. It creates an informed initial guess for an interior transfer in the CR3BP model by selecting orbits from the $L_2$ S halo and the $P_2$ DRO families of orbits, and delivers a mass-optimal solution, that utilizes the minimum possible number of intermediate arcs. The CR3BP solution is fed as the initial guess for converging the interior trajectory in the higher-fidelity ephemeris

model. The mass-optimal interior solution is depicted in Figures 9 (a)-(c) for representations in three different frames, with varying central bodies. Red arcs in the figures correspond to thrusting segments, while the arcs represent the times at which LIC is coasting.

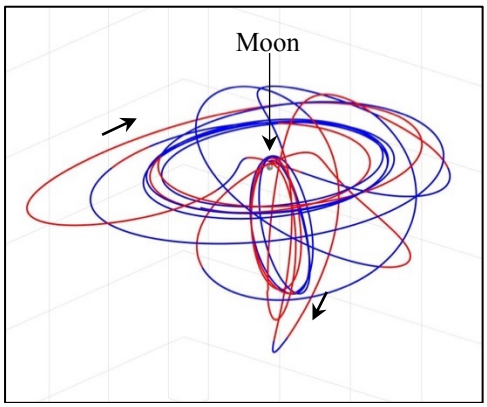


(a) Interior transfer in the ephemeris model Earth-Moon barycentric rotating frame

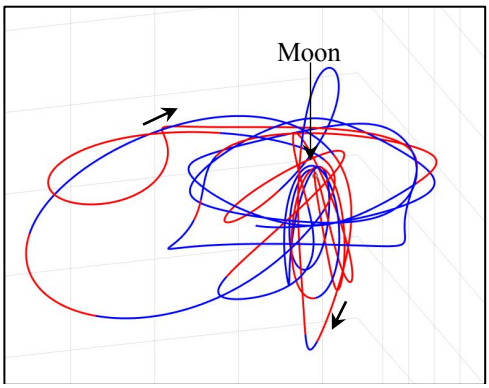


(b) Interior transfer in the ephemeris Moon-centered J2000 ecliptic frame

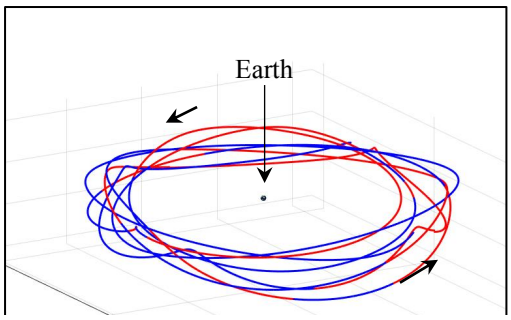


(c) Interior transfer in the Earth-centered J2000 ecliptic frame

Fig. 9. Interior transfer from the $L_2$ S 9:2 NRHO science orbit to a $P_2$ DRO in the ephemeris model. Red and blue represent thrust and coast segments respectively

For the case of the interior transfer, the spacecraft requires 118.7911 days to travel from the departure to the arrival orbit, while consuming 0.2647 kg of the 13.6 kg of the remaining spacecraft mass from phases I and II. A second strategy in the trajectory design framework of LIC's phase III explores the generation of exterior-type transfers, by utilizing nearby structures that depart the vicinity of the Earth-Moon system. Such is the case of some of the exterior resonant orbits that exist within the context of the CR3BP force model.

One of the most common approaches to generate these resonant orbits consist of correction strategies and/or continuation methods, to transform a two-body resonant periodic orbit into the three-body model. Within the context of the Earth-Moon CR3BP force model, a spacecraft is defined to be in $p{:}\,q$ resonance with the Moon, if it completes $p$ orbits with respect to the Earth in the same time interval in which the Moon achieves exactly $q$ orbits [17,18]. In this definition, $p$ and $q$ are two positive integers. Employing a continuation method, a family of resonant orbits is generated, and similar to the families of libration point orbits, may offer useful options for constructing trajectories in more complex scenarios [18].

A 3:4 resonant arc is then utilized to generate an informed initial guess for constructing an exterior trajectory from the $L_2$ S 9:2 NRHO science orbit to the 70,000km-altitude DRO. The spatial configuration of the aforementioned resonant family, as well as its energy parametrization across all different members of the family depicted in Figure 10, offer suitable candidates for the initial guess generation of the exterior transfer. Even though many resonant families do exist within the CR3BP force model, the 3:4 family is chosen due to its wide range of energy span, as well as its three-dimensional reach in configuration space, which is advantageous when constructing initial guesses for transfers between highly inclined (i.e., out-of-plane) orbits.

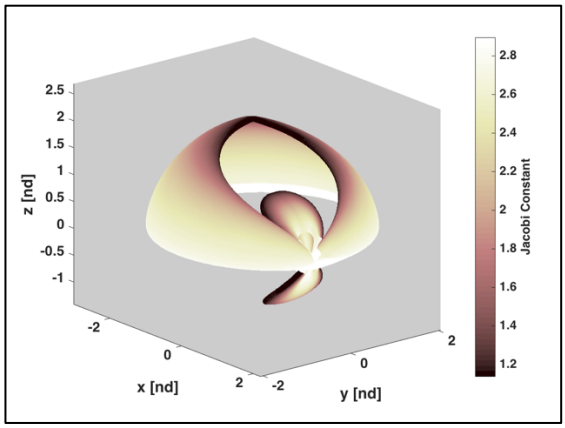


Fig. 10. 3:4 spatial resonant family of orbits in the Earth-Moon CR3BP model

The initial guess is converged and optimized in the lower-fidelity CR3BP force model, and that solution is later utilized to generate the exterior ephemeris mas-optimal trajectories in Figures 11 (a)-(c), where its representation as seen by different observers is depicted. As expected, LIC departs the vicinity of the Moon to accomplish the required plane and energy changes, to later re-enter the system and arrive on its destination orbit. Majority of the thrusting happens away from the lunar region.

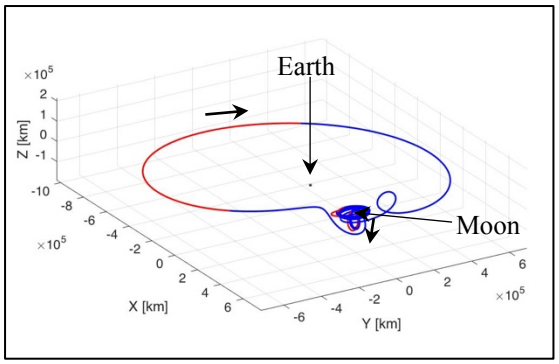


(a) Exterior transfer in the Earth-Moon barycentric rotating frame

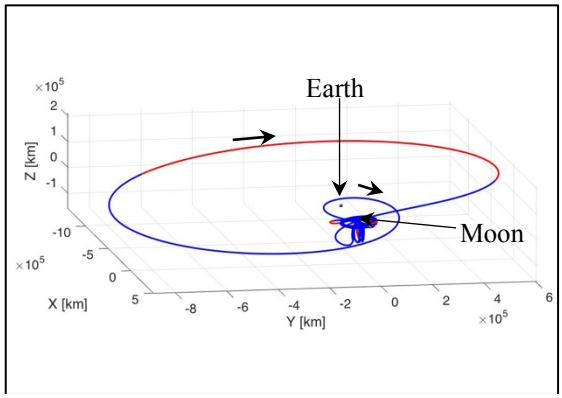


(b) Exterior transfer in the ephemeris Moon-centered J2000 ecliptic frame

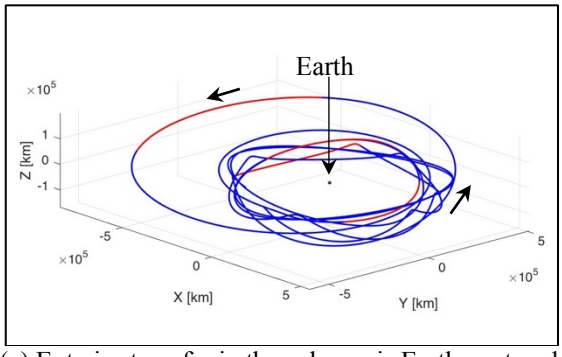


(c) Exterior transfer in the ephemeris Earth-centered J2000 ecliptic frame

Fig. 11. Exterior transfer from the $L_2$ S 9:2 NRHO science orbit to a $P_2$ DRO in the ephemeris model. Red and blue represent thrust and coast segments, respectively

For the case of the exterior-type transfers, LIC requires 110.1077 days to travel from the science orbit to the DRO, and, it consumes about 0.1481 kg of the remaining 13.6 kg mass.

### *4.3.2 Phase III.2: Transfer from a NRHO to a 'Flat' Halo Orbit*

As a second extended option for the LIC spacecraft, this investigation studies the design of a low-thrust spacecraft trajectory from a $L_2$ S 9:2 NRHO to a Northern (N) 'flat' halo orbit in the vicinity of the $L_2$ libration point. Even though the arrival halo orbit is unstable in the Lyapunov sense, which suggest the existence of manifold structures leaving to and from the periodic orbit, the energy-informed adaptive algorithm is once again leveraged to construct an interior-type initial guess, that is corrected in the lower-fidelity CR3BP model, utilizing the minimum number of intermediate orbits required to travel from departure to destination.

The CR3BP mass-optimal solution is re-converged in the ephemeris model for a November 1st, 2022 selected epoch. This epoch is chosen from the roughness parameter technique, to enable LIC to complete its primary mission around the $L_2$ S 9:2 NRHO science orbit. Figures 12 (a)-(c) represent the mass-optimal solution corrected in a higher-fidelity ephemeris model, for an observer fixed in three different reference frames. The trajectory design framework selects the use of the sliding algorithm over the use of manifold structures, to guarantee that the spacecraft does not exhibit long transits around the Earth-Moon system.

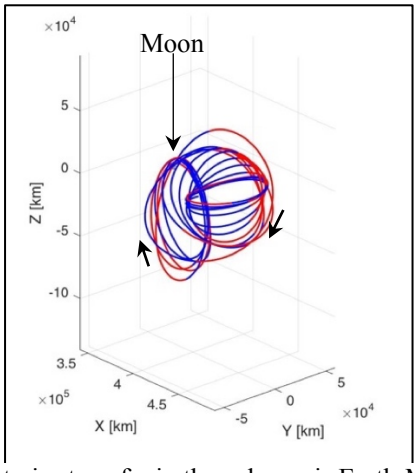


(a) Interior transfer in the ephemeris Earth-Moon barycentric rotating frame

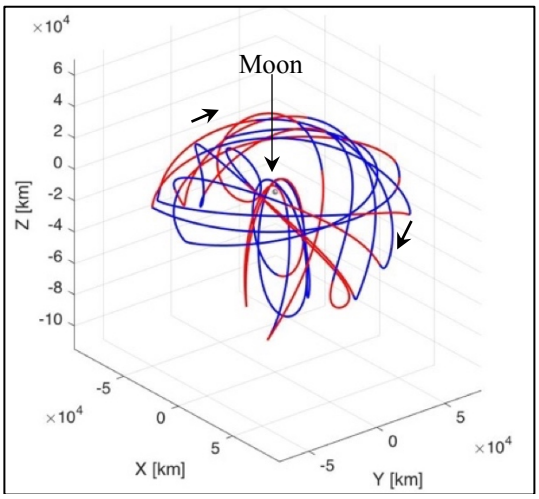


(b) Interior transfer in the ephemeris Moon-centered J2000 ecliptic frame

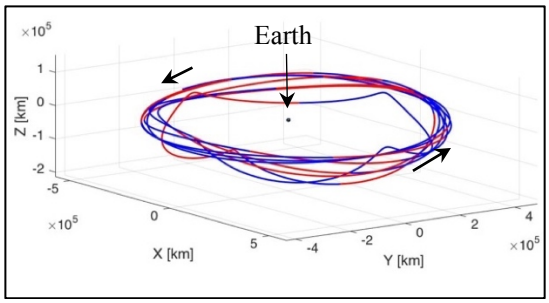


(c) Interior transfer in the ephemeris Earth-centered J2000 ecliptic frame

Fig. 12. Interior transfer from the $L_2$ S 9:2 NRHO science orbit to a $L_2$ 'flat' halo orbit. Red and blue represent thrust and coast segments respectively

For all three observers, it is seen that the spacecraft does not depart the vicinity of the Moon, behavior that is consistent with that of interior-type transfer trajectories. For each of the plots in Figure 12, the red portions of the transfer represent segments where the thrust is active, while the blue arcs correspond to segments where the spacecraft's engine is turned off. LIC performance for this potential extended mission interior transfer requires 164.1934 days of transit from the departure to the arrival orbits, and it consumes 0.3046 kg of propellant.

An exterior-type transfer is also generated for the case of LIC traveling from the $L_2$ S 9:2 NRHO science orbit to a $L_2$ 'flat' halo orbit. In this scenario, it is noted that the arrival orbit is unstable in the Lyapunov sense, hence, it does possess natural structures that depart and arrive into the orbit in a ballistic fashion. These structures are computed via invariant manifold theory, and along with a Poincaré mapping technique, are utilized to construct initial guesses for the exterior transfers in the CR3BP force model.

Once the initial guess is converged as a mass-optimal continuous solution in the lower-fidelity model, this result is fed into the higher-fidelity ephemeris dynamics as initial guess, producing the exterior-type transfers shown in Figures 13 (a)-(c), where the motion is visualized as seen from an observer placed in three different reference frames. In this case, LIC requires 106.4887 days to travel from the departure primary mission science orbit to the arrival orbit near the $L_2$ libration point. The propellant consumption is such that 0.1745 kg of the phase II 13.6 kg remaining are consumed.

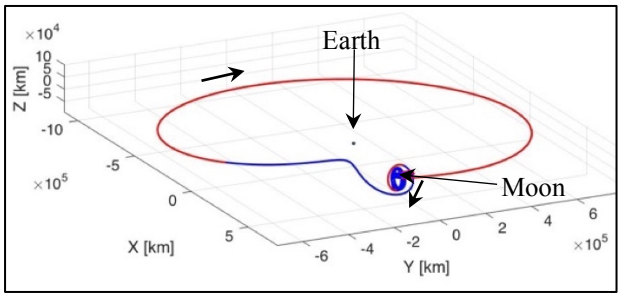


(a) Exterior transfer in the ephemeris Earth-Moon barycentric rotating frame

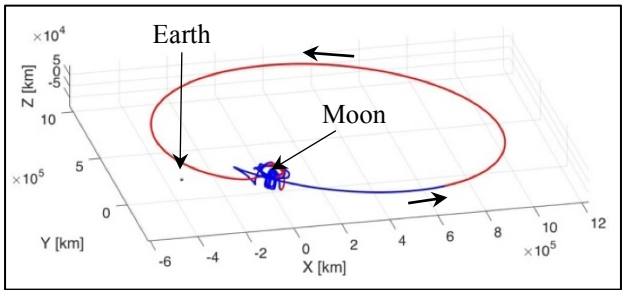


(b) Exterior transfer in the ephemeris Moon-centered J2000 ecliptic frame

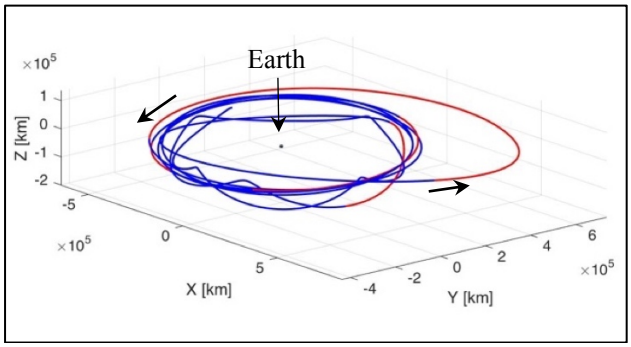


(c) Exterior transfer in the ephemeris Earth-centered J2000 ecliptic frame

Fig. 13. Exterior transfer from the $L_2$ S 9:2 NRHO science orbit to a $L_2$ 'flat' halo orbit in the ephemeris model. Red and blue represent thrust and coast segments, respectively

#### *4.3.3 Phase III.3: Transfer from a NRHO to a Low Lunar Elliptical Orbit (LLO)*

The final potential extended mission scenario studied in this investigation, considers transferring LIC from the $L_2$ S 9:2 NRHO science orbit to a low lunar elliptical orbit with a 100km periapsis altitude and a 5,000 km apoapsis altitude. The full set of Keplerian orbital elements that defined the arrival orbit are summarized in Table 2. An interior-type transfer is sought from the generalized trajectory design framework.

Table 2. Summary of Keplerian orbital elements defined in a Moon-centered inertial frame for the selected arrival low lunar elliptical orbit

| Orbital Elements | Value |
|---|---|
| Semi-Major Axis, $a$ | 4,287.4 $km$ |
| Eccentricity, $e$ | 0.5714 |
| Inclination, $i$ | $56^o$ |
| RAAN, Ω | $65^o$ |
| Argument of Periapsis, $\omega$ | $355^o$ |

The orbital inclination is measured relative to the Moon's equator and the right ascension of the ascending node (RAAN) is defined with respect to the vernal equinox vector. The main challenge encountered on the design of this trajectory is derived from the large energy gap between the departure and arrival orbits. Furthermore, the energy-informed adaptive sliding algorithm needs to accommodate that the two orbits exist in different dynamical models, as the departure orbit resides within the context of the CR3BP force model, while the arrival orbit is a Keplerian conic defined in the context of the 2BP.

The first step in the trajectory design framework is then to transform the Keplerian orbit to its correspondent trajectory in the CR3BP force model, as sown in Figure 14, where it is seen that the LLO is no longer a conic section nor it is a periodic orbit [19]. The path is propagated for 160 revolutions of the original Keplerian orbit, whose orbital period is of about seven hours.

Once the arrival orbit is transformed into CR3BP coordinates, the trajectory design is split into two steps:

1. Backwards propagation with a suboptimal thrust spiral from the LLO until the trajectory crosses a selected surface of section in the lunar region
2. Slide through a number of intermediate members of the $L_2$ S halo family, until the energy of the intermediate orbit matches the energy of the thrust spiral trajectory on the surface of section

The initial guess constructed from this design methodology in the CR3PB is depicted in Figure 15. The energy-informed adaptive sliding algorithm suggests that three members of the southern halo family of orbits near the $L_2$ libration point, be incorporated from the orbit chaining framework.

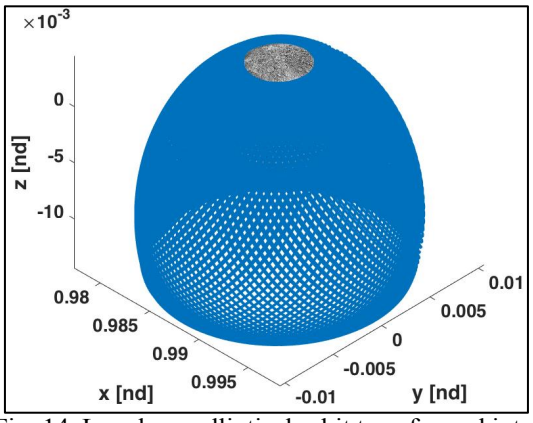


Fig. 14. Low lunar elliptical orbit transformed into the CR3BP dynamical model

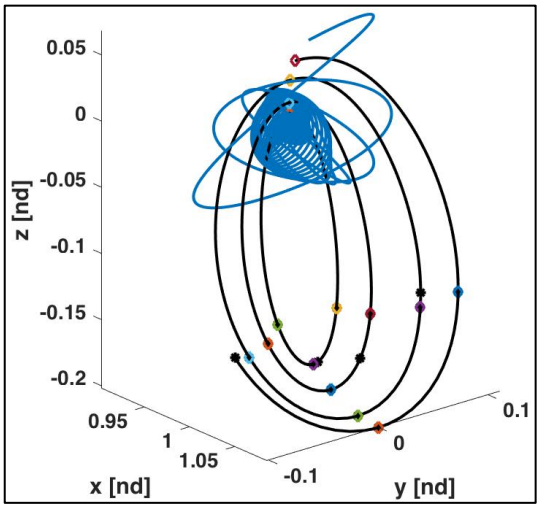


Fig. 15. Initial guess for the interior trajectory from the NRHO science orbit to the arrival LLO in the CR3BP dynamical model

To fully generate a converge solution, it is necessary to link steps 1. and 2. from the trajectory design process, by means of a differential corrections scheme, that delivers an interior-type path continuous in position, velocity and mass states. Such solution is represented in Figure 16 for the CR3BP force model, where the red and blue arcs correspond to thrust and coast segments, respectively. The spacecraft requires 72.9701 days to travel from the departure to the destination orbit, and it consumes about 0.4671 kg of the remaining propellant mass from LIC's phases I and II primary mission. The solution in Figure 16 is a mass-optimal trajectory. By utilizing the roughness parameter technique, a departure epoch of September 1st, 2022 is selected to transition the CR3BP solution into a higher-fidelity trajectory, depicted

in Figures 17 (a)-(c), for an observer fixed in three different reference frames.

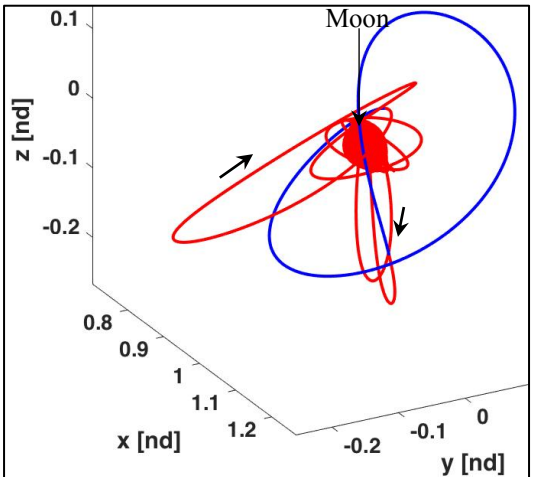


Fig. 16. Converged solution for the interior trajectory from the NRHO science orbit to the arrival LLO in the CR3BP dynamical model. Red and blue represent thrust active and engine off, respectively

In all three plots for the different central bodies and reference frames in Figure 17, it is observed that the energy-informed adaptive sliding algorithm is successful in producing a mass-optimal solution in the higher-fidelity ephemeris model that does not need to depart the Earth-Moon system to accomplish the required change in energy. The LIC spacecraft requires 66.0889 days to travel from the $L_2$ S 9:2 NRHO science orbit to the low lunar elliptical arrival orbit, and it consumes 0.5356 kg of propellant from the 13.6kg remaining from phases I and II.

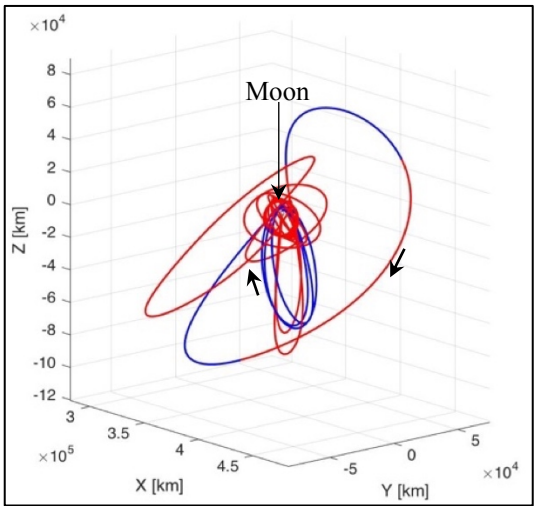


(a) Interior trajectory in the ephemeris Earth-Moon barycentric rotating frame

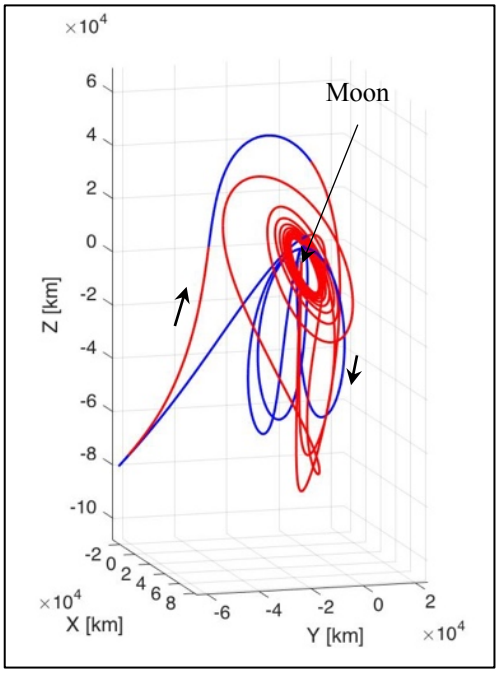


(b) Interior trajectory in the ephemeris Moon-centered J2000 ecliptic frame

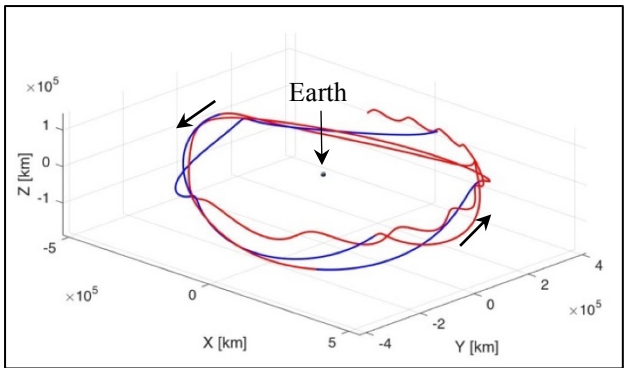


(c) Interior trajectory in the ephemeris Earth-centered J2000 ecliptic frame

Fig. 17. Interior transfer from the $L_2$ S 9:2 NRHO science orbit to a low lunar elliptical orbit in the ephemeris model. Red and blue represent thrust and coast segments respectively

### *4.3.4 LIC Phase III: Summary of Potential Extended Mission Options*

Table 3 depicts a summary of the results obtained in this investigation, for a variety of sample candidate transfer options for the Lunar IceCube spacecraft, after the completion of its primary science and technology demonstration mission objectives. All interior transfers are generated utilizing an energy-informed adaptive sliding algorithm and optimized for propellant consumption in a higher-fidelity ephemeris model that

includes the point mass gravitational acceleration of the Sun, the Earth and the Moon. Furthermore, all interior and exterior trajectories are evaluated for a range of different epochs starting in March 1st, 2022, epoch after which LIC would have already arrived in its primary science mission orbit. By leveraging the roughness parameter technique, via measurement of the RMS value of the position profile of each initial guess trajectory for every epoch in consideration, a departure epoch from the $L_2$ S 9:2 NRHO science orbit was selected for each transfer scenario. All transfers constructed with this trajectory design framework meet the propellant and time-of-flight requirement for possible extended mission options for the Lunar IceCube spacecraft.

Table 3. Summary of results for Phases III of LIC potential extended mission options trajectories from the primary science mission orbit

| Orbit | Type | $\Delta m\ [kg]$ | $ToF\ [days]$ |
|---|---|---|---|
| DRO | Interior | 0.2647 | 118.7911 |
| | Exterior | 0.1481 | 110.1077 |
| 'Flat' halo | Interior | 0.3046 | 164.1934 |
| | Exterior | 0.1745 | 106.4887 |
| LLO | Interior | 0.5356 | 66.0889 |

## 6. Concluding Remarks

This investigation presents a framework for constructing lunar IceCube (LIC) trajectories from the Earth deployment to a final science orbit, while exploring a variety of potential destination orbits to be considered for its extended mission applications. The approach utilizes dynamical structures available in the BCR4BP, as well as in the CR3BP force models, along with the robust properties of direct optimization strategies to create a trajectory design framework capable of addressing the LIC spacecraft's limited control authority and need for adaptability.

Dividing the trajectory design framework into distinct phases eases the design challenge by permitting solutions to each phase to be developed largely independently of one another, while continuously tracking propellant consumption and time-of-flight requirements of each phase.

This procedure is adaptable to changes in launch date and generates transfers that fall within the time of flight and propellant mass requirements allotted to each phase of the LIC mission. Lastly, the proposed framework is applicable to other small satellite missions that will be deployed as secondary payloads on launches similar to Artemis-1. Its utility reaches well beyond the present applications.

## Acknowledgements

The authors would like to thank the school of Aeronautics and Astronautics Engineering at Purdue University for use of computing resources, as well as the members of the Multibody Dynamics Research Group at Purdue University. Portions of this work were supported by the Purdue University Minority Engineering Program. The authors also appreciate partial support from NASA Grant 80NSSC20K1117

## References

[1] D. C. Folta, N. Bosanac, A. D. Cox, and K. C. Howell. "The Lunar IceCube Mission Design: Construction of Feasible Transfer Trajectories with a Constrained Departure". Advances in the Astronautical Sciences, 158:1369–1387, 2016

[2] R. Pritchett, A. D. Cox, K. C. Howell, D. C. Folta, and D. Grebow. "Low-Thrust Trajectory Design Via Direct Transcription Leveraging Structures from the Low-Thrust Restricted Problem". In 69th International Astronautical Congress, pages 1–16, Bremen, Germany, 2018.

[3] R. E. Pritchett, K. C. Howell, and D. J. Grebow. "Low-Thrust Transfer Design Based on Collocation Techniques: Applications in the Restricted Three-Body Problem". In AAS/AIAA Astrodynamics Specialist Conference, Stevenson, Washington, 2017.

[4] K. K. Boudad. "Disposal Dynamics from the Vicinity of Near Rectilinear Halo Orbits in the Earth-Moon-Sun System". Master's Thesis, Purdue University, 2018.

[5] Prado Pino, B., and Howell, K. C., "An Energy-Informed Adaptive Algorithm for Low-Thrust Spacecraft Cislunar Trajectory Design", ASS/AIAA Astrodynamics Specialist Conference, Lake Tahoe, California (Virtual), August 9-12, 2020

[6] Boudad, K. K., Howell K.C., and Davis, D. C., "Near Rectilinear Halo Orbits in Cislunar Space Within the Context of the Bicircular Four-Body Problem", 2nd IAA/AAS SciTech Forum, Moscow Russia, June 25-27, 2019

[7] NASA JPL-Navigation and Ancillary Information Facility. An Overview of Reference Frames and Coordinate System sin the SPICE Context. https://naif.jpl.nasa.gov/pub/naif/toolkit_docs/Tutorials/pdf/individual_docs/17_frames_and_coordinate_systems.pdf, Last Accessed Date: [20 July 2020].

[8] NASA JPL-Navigation and Ancillary Information Facility. The SPICE Toolkit. https://naif.jpl.nasa.gov/naif/toolkit.html, Last Accessed Date: [4 July 2020]

[9] Ashwati Das-Stuart. "Artificial Intelligence Aided Rapid Trajectory Design in Complex Dynamical Environments". Ph.D. Dissertation,

Purdue University, West Lafayette, Indiana, 2019

[10] E. S. Gadelmawla, M. M. Koura, T. M. A. Maksoud, I. M. Elewa, H. H. Soliman. "RoughnessParameters." *Journal of Materials Processing Technology*, 123, 2002, pp. 133-145

[11] N. Bosanac, A. D. Cox, K. C. Howell, and D. C. Folta. "Trajectory Design for a Cislunar Cubesat Leveraging Dynamical Systems Techniques: The lunar IceCube Mission". In 27th AAS/AIAA Space Flight Mechanics Meeting, San Antonio, Texas, February 2017.

[12] Koon, W.S., Lo, M.W., Marsden, J.E. and Ross, S.D. "Three Body Problem and Space Mission Design". Springer-Verlag, 2006

[13] Marchand, B. "Temporary Satellite Capture of Short Period Jupiter Family Comets from the Perspective of Dynamical Systems". M.S. Thesis, Purdue University, West Lafayette, Indiana, 2000

[14] Henri Poincare. "Les Methodes Nouvelles de la Mecanique Celeste", No 2, Gauthier-Villars, Paris, 1893

[15] R. Pritchett, "Strategies for Flow-Thrust Transfer Design Based on Direct Collocation Techniques", Ph.D. Dissertation, Purdue University, West Lafayette, Indiana, 2020

[16] R. Mathur. "Low Thrust Trajectory Design and Optimization: Case Study of a Lunar CubeSat Mission". In 6th International Conference on Astrodynamics Tools and Techniques, pages 1–11, Darmstadt, Germany, 2016. Emergent Space Technologies, Inc

[17] Szebehely, V. "Theory of Orbits: The Restricted Problem of Three Bodies". Yale Univ New Haven, CT, 1967

[18] Vaquero, M. and Howell, K.C. "Leveraging Resonant Orbit Manifolds to Design Transfers between Libration Point Orbits in Multi-Body Regimes". *Journal of Guidance, Control and Dynamics*, 37(4), 2014, pp. 1143-1157

[19] Grebow, D. J., Ozimek, M. T. and Howell, K. C. "Design of Optimal Low-Thrust Lunar Pole-Sitter Missions. *The Journal of the Astronautical Sciences*, 58(1), 2011, pp.55-79.